Senescent cells deposit intracellular contents through adhesion-dependent fragmentation

Matej Durik[1,2,3,4,5], Daniel Sampaio Gonçalves[1,2,3,4], Coralie Spiegelhalter[1,2,3,4], Nadia Messaddeq[1,2,3,4], and William M. Keyes[1,2,3,4,5,]

[1]Institut de Génétique et de Biologie Moléculaire et Cellulaire (IGBMC), Illkirch, France.
[2]UMR7104, Centre National de la Recherche Scientifique (CNRS), Illkirch, France.
[3]U1258, Institut National de la Santé et de la Recherche Médicale (INSERM), Illkirch, France.
[4]Université de Strasbourg, Illkirch, France

Keywords: senescence, damage, debris, aging, adhesion, DAMPs,

[5]Correspondence to

Bill Keyes,
IGBMC,
1 Rue Laurent Fries, BP 10142,
67404 Illkirch - CU Strasbourg
France

e-mail: bill.keyes@igbmc.fr

Matej Durik,
IGBMC,
1 Rue Laurent Fries, BP 10142,
67404 Illkirch - CU Strasbourg
France

Email : durikm@igbmc.fr

ABSTRACT

Cellular senescence is a complex cell state with roles in tumor suppression, embryonic development and wound repair. However, when misregulated, senescence contributes to aging and disease. Here we identify that senescent cells generate/break off large membrane-bound fragments of themselves through cell-to-cell adhesion. We designate these as senescent-cell adhesion fragments (SCAFs) which were present in all types of senescent cell examined. We show they contain many organelles from the original cell, but without nuclear material. Quantitative and dynamic profiling shows that SCAFs are large, may persist for a number of days, but rupture and release their contents onto neighboring cells. Protein profiling identifies that SCAFs contain a complex proteome including immune recruitment factors and damage-associated molecular patterns (DAMPs). Functional studies reveal that SCAFs activate signatures related to wound healing and cancer, and promote invasion and migration. Altogether, we uncover an additional cellular feature of senescent cells, by which they deposit intracellular contents on other cells. We speculate this may aid in boosting immune responses, but in chronic situations, may contribute to debris buildup, inflammaging and age-associated changes.

INTRODUCTION

Cellular senescence is a highly dynamic and complex cellular response that can affect all stages of life (1,2). Senescence is triggered in response to replicative exhaustion, oncogene activation, chemotherapy and various cellular stresses, but it can also be induced in a controlled manner via specific signaling pathways in the context of regeneration or embryonic development (1,3–5). Two main characteristics of senescent cells are an irreversible proliferative arrest and a highly active secretory profile called the senescence-associated secretory phenotype (SASP) (4,6). The SASP consists of many signaling molecules such as chemokines, growth factors and extracellular matrix remodelers and it has a variety of functions and effects on neighboring tissue (7,8).

The outcome of senescence induction can either be beneficial, or detrimental for the organism, depending on timing and context. Senescence plays key physiological roles during embryonic development, wound healing, reprogramming and regeneration (9–13). Here, senescent cells appear transiently, and through the SASP, contribute to tissue patterning and regeneration, cell plasticity, growth and repair. Critically, one of the best studied functions of the SASP is the recruitment and instruction of immune cells, including macrophages and neutrophils, to remove senescent cells (8,14,15).

Conversely, the aberrant induction or chronic persistence of senescent cells is generally detrimental for the organism, and is linked to aging, cancer and other disease states. During aging, the accumulation of senescent cells actively contributes to tissue aging (16,17). In addition, many age-related diseases have an increased senescent cell burden, ranging from idiopathic pulmonary fibrosis (IPF) and arthritis, to Alzheimer's and Parkinson's disease (3,18–20). Senescent cells also significantly impact cancer formation, promoting tumor cell proliferation, recurrence after treatment and metastasis (5,21). During recent years, numerous studies have identified how the elimination or removal of senescent cells in aged or damaged tissues can be beneficial for tissue function. Genetic ablation of senescent cells in aged mice was shown to improve health span and prolong lifespan (16). Such initial genetic studies spurred the search for drugs and compounds to remove or interfere with senescence (senolytics and senomorphics, respectively) (3,22). Many studies have now identified how such compounds can decrease senescence burden, and alleviate aging features and many disease states where senescence has been identified. Therefore, aberrant induction of senescence is detrimental, and interfering with it can have a beneficial impact on aging and age-related diseases.

However, exactly how cellular senescence contributes to aging or pathology remains unclear. On one hand, the accumulation of non-proliferating cells can perturb tissue homeostasis and stem cell function, preventing cell turnover and tissue repair (23). On the other hand, persistent SASP signaling can dysregulate the surrounding tissue. Senescence is also thought to contribute to the process of inflammaging, a chronic inflammation in aged tissues in which persistent recruitment of activated immune cells decreases tissue function and promotes disease (24,25). Inflammaging is thought to primarily arise from cellular debris, including misplaced or misfolded self-molecules that are released from dead or damaged cells, and which collectively are referred to as damage-associated molecular patterns (DAMPs) (25). Interestingly, it was shown that senescent cells can secrete some DAMPs, including HMGB1, supporting the link that senescent cells can contribute to the inflammaging process (7,26). However, as most classical DAMPs are not typical SASP factors, exactly how senescence may be linked to inflammaging is not clear.

As such, there is critical need to better understand the cellular mechanisms of senescence, how it functions, and how its misregulation contributes to aging and disease. Here, we identify a striking new feature of senescent cells, where they generate and break off large fragments of themselves, through cell-cell adhesion. We demonstrate that these fragments ultimately rupture and deposit their large cargo of intracellular contents onto neighboring cells. In functional studies, we show that among the proteins released are many DAMPs, and that

senescent fragments can induce proliferation, invasion and migration. We believe senescent fragments are yet another critical step towards our understanding of the senescence program.

RESULTS

Cellular senescence is a highly dynamic process. Following induction, cells express key markers and features of senescence at different stages. In a typical scenario of senescence induction in cells in culture by 10Gy irradiation, entry into a senescent state occurs over time. First, cells begin to express early features of senescence, such as decreased proliferation and induction of p21, typically within 24 hours (Supp. Fig 1). Afterwards, senescence-associated beta-galactosidase (SA-β-gal) is detectable from approx. 3 days. Then p16 expression, often used as a surrogate marker for senescence, becomes detectable at later stages (Supp. Fig 1). Our interest was to study the dynamic process of senescence onset and maintenance. To achieve this, we established an *in vitro* model system that would enable us to image and track individual cells becoming senescent over time (Figure 1A). This involved infecting human IMR90 fibroblasts with a constitutive GFP-expressing retroviral vector (MSCV-PIG), so that after drug selection, these cells would stably express GFP. Using these GFP-positive fibroblasts, we then either induced senescence by irradiating with 10Gy X-ray irradiation, or left the cells proliferating as controls. Next, either proliferating or irradiated GFP-positive cells were diluted at a ratio of 1:1000 into either proliferating or senescing cells that were negative for GFP (NEG) to achieve the following combinations: proliferating-GFP into proliferating-NEG; senescing-GFP into proliferating-NEG; senescing-GFP into senescing-NEG (Figure 1A). We reasoned that in such a scenario, the proliferating-proliferating (Prol-Prol) conditions would resemble normal healthy conditions, the senescing into proliferating (Sen-Prol) would resemble low levels of senescence induction, while the senescing into senescing (Sen-Sen) would more closely resemble standard senescent culture conditions, or chronic senescent buildup as seen in damaged and aged tissue.

Following irradiation and plating in the various conditions, we imaged the cells each day. Unexpectedly, by 3-5 days post-irradiation, we repeatedly observed small GFP positive fragments in the cultures of cells induced to senesce, in both the proliferating and senescing environments (Figure 1B). These were not visible, or were only present at very low levels in the proliferating control conditions. However, when we imaged these fragments at higher resolution, it was clear they were not pieces of cell debris in the media, but were GFP-cellular fragments bound to the membranes of adjacent cells (Figure 1C). To determine the origin of these fragments, we next performed time-lapse imaging of the different culture conditions between days 0 and 3, when fragments were first detectable. In all conditions, cells routinely made contact points with neighboring cells in a dynamic manner. In control cells (Prol-Prol),

these contacts were non-permanent. Somewhat surprisingly, the senescent cells also exhibited quite dynamic behavior, moving around the dish and making contacts. However, in cells induced to become senescent, these contacts persisted and the cells frequently remained attached as the cells moved apart (Figure 1D). This movement resulted in the generation of long GFP-positive threads pulled between two cells, undergoing stretching and tension. Then, at one point, the senescent cells tore, leaving large GFP-positive fragments attached to the neighboring cell (Figure 1D). Surprisingly however, during this process, both the fragments and the senescent cells remained intact, suggesting there are active membrane repair mechanisms present. It appears that the strength of adhesion is quite high, as in some cases, there was clear recoil of the senescent cell following generation of the fragment. This process of adhesion-mediated fragmentation was consistently observed. We quantified the number of fragments at early timepoints, and found these became detectable around 3 days following irradiation, increasing to approx. 10-12 fragments per senescent cell at day 5 (Figure 1E). This process of fragmentation continued, and similar numbers of fragments were seen at later stages in fully senescent cells (Figure 1E). Together, this demonstrates that fragmentation is an ongoing and active process associated with senescent cells.

Next, we used image-analysis to quantify the fragment sizes. As these are dynamically-forming structures, there was great variation in the major-axis length, with some fragments stretching along the neighboring cell, while others had already recoiled to a smaller size (Figure 1F). Overall however, this demonstrated that fragments are large structures with a mean length of the major axis of 7-8um (Figure 1G).

To investigate if cell-cell adhesion is required for this process, we next plated GFP-positive senescing cells at low density, in the absence of neighboring cells. These cells displayed similar senescent features as the previous conditions, but did not generate fragments (Figure 1H). Together, this uncovers that senescent cells generate large cell fragments through a process of cell-cell adhesion. As a result, we chose to call these “senescent-cell adhesion fragments” (SCAFs).

As such cellular fragments had not previously been associated with senescent cells, we asked if they were unique to irradiation-induced senescence (IIS) in IMR90 primary human fibroblasts. To address this we examined other conditions, including oncogene-induced senescence (OIS) in primary fibroblasts, or IIS or chemotherapy-induced senescence (TIS) in human liver cancer cells (Figure 1I). in each case, SCAFs were detectable attached to neighboring cells. Similar fragments were also detected in mouse primary dermal fibroblasts and mouse primary keratinocytes, following irradiation or oncogene expression while absent

in proliferating cells (not shown). Therefore, in every situation examined, senescent cells were found to undergo fragmentation.

To further explore whether SCAFs are a defined structure associated with senescent cells, we wanted to examine if they are a feature of senescent cells *in vivo*. To address this, we used a model of oncogene-induced senescence in mouse hepatocytes (14). Here, hydrodynamic tail-vein injection is used to deliver two plasmids, one with transposase and the other carrying a transposon with oncogenic $NRas^{G12V}$-GFP or inactive $NRas^{G12V/D38A}$-GFP. This results in construct expression in individual hepatocytes in the liver (Figure 2A). In this setting, the hepatocytes expressing oncogenic Ras undergo senescence, while the inactive Ras-infected cells remain proliferative, but in each case the infected cells are GFP-positive. The infected cells can then be identified with immunostaining for GFP, and additionally with senescence markers such as SA-β-gal for the senescent cells (Figure 2A).

Next, on thick sections of liver containing the proliferating control or the senescent hepatocytes, we performed immunostaining and imaging of GFP, generating image stacks (Figure 2B). The control cells expressing inactive Ras-GFP clearly retained the epithelial shape of the hepatocytes, whereas the senescent cells displayed a much more irregular shape, projecting many branches, as well as scattered non-connecting fragments (Figure 2B). To determine whether these fragments were indeed separate from the senescent cells, or remained connected, we performed confocal imaging, and generated 3D reconstructions. In each sample analyzed (n=3 livers), SCAFs were detectable adjacent to, but not connected to, the senescent cells, while none were obvious in the controls (Figure 2C, D). These results demonstrate that senescent cells *in vivo* generate SCAFs.

By imaging SCAFs in culture, we observed that these presented as large fragments of senescent cells that formed by attachment to neighboring cells. We wanted to further analyze the structure of these bodies, and performed correlative light and electron microscopy (CLEM) analysis. As before, we plated senescing GFP-positive cells in an environment of GFP-negative senescing cells (Sen-Sen), and at 5 days post irradiation, analyzed the cells. Fluorescence and phase contrast imaging allowed us to identify and localize SCAFs of various sizes (Figure 3A, B), and these samples were subsequently processed for EM analysis. The same fragments were readily identified at the ultrastructural level (Figure 3C). In each case, the SCAFs appeared as large membrane-bound bodies, filled with cytoplasm. They contained a variety of organelles, including mitochondria, smooth endoplasmic-reticulum, and clathrin vesicles, as well as lipid droplets, autophagosomes and residual bodies (Figure 3D). In most fragments, ribosomes were also clearly visible. In some instances, adherens junctions were

also visible at the site of adhesion between the SCAF and the neighboring cell, further supporting that SCAFs are generated by cell-cell adhesion (Figure 3D, E). Interestingly, we were unable to detect nuclei or nuclear material in any of the SCAFs analyzed, suggesting this is excluded from these structures. Altogether, the SCAFs appeared as large intact and detached pieces of the original senescent cell, adhered to an adjacent cell.

To further investigate their structure and function, we devised a strategy to collect SCAFs through enzymatic dissociation and fluorescence-activated cell sorting (FACS) isolation (Figure 4A). First, we isolated SCAFs and performed cytospin analysis, attaching the GFP-positive cells or SCAFs on glass slides (Figure 4B). When immuno-stained for GFP and stained with DAPI to detect nuclei, we could not detect DAPI signal in the SCAFs, supporting our EM analysis that SCAFs do not contain nuclear material. Analysis of the size of these sorted SCAFs demonstrated they are similar to those in situ (Supp Figure 2).

As the cell membrane of the SCAFs remain intact during their genesis, we wanted to explore the fate of these structures, and how long they persisted. To achieve this, we added the isolated SCAFs to cultures of proliferating IMR90 fibroblasts, to track their behavior and dynamics (Figure 4C). Interestingly, most SCAFs remained intact throughout the procedure, and when plated in culture, they exhibited random dynamic behavior, which included spinning, projecting and retracting arms, or crawling-like behavior. To determine how long the SCAFs persisted, we performed quantitative analysis and imaging over time, following their addition to cultures (Figure 4D). During the first day, most SCAFs appeared intact, and tended to adhere to the cells in culture. By two days, there was a noticeable decrease in the number of SCAFs, but those remaining still clustered on cells. By three days, most of the GFP signal had disappeared, but any remaining signal was frequently attached to cells, in what appeared to be clusters of cellular debris (Figure 4D). Imaging of individual SCAFs at these later timepoints showed that many of them were bursting, or undergoing lysis, and releasing their contents onto the neighboring cell, while losing GFP-signal (Figure 4E). This suggests that SCAFs can remain intact for a period of time, but that their lysis results in the generation of debris on the surface of the cell to which they are attached. To further test this, we repeated the sorting and addition of SCAFs to cultures, but this time adding higher numbers of SCAFs to the recipient cultures. As expected, after 3 days, this clearly resulted in large extra-cellular debris deposits (Figure 4F).

These results suggest that SCAFs spill their contents onto the neighboring cells, and as such could suggest novel means of senescent cell communication. We speculated that the intracellular proteins might persist outside the cell longer than the GFP signal used to identify

the SCAFs. To test this, we used a method to label the protein contents of the senescing cells from which the SCAFs were isolated. We added L-Homopropargylglycine (L-HPG), a synthetic alternative to methionine that is randomly incorporated during protein translation, and which can then be detected with Click-chemistry. In this way, the protein content of senescing cells can be subsequently visualized. As before, SCAFs were isolated from day 5 irradiated GFP-positive cells that were treated with L-HPG, and these were added to proliferating IMR90 fibroblasts for two days. As before, much of the GFP signal had disappeared, and large residual clumps of debris persisted. Next, these cells were stained using the click-reaction and immuno-stained for GFP, to visualize the protein content of the SCAFs. As expected, even though the GFP signal had mostly disappeared, now it was obvious that the spilled protein contents remained on the treated cells (Figure 4G). Interestingly, in some cases, intracellular staining was evident, presenting as small regular dots, suggesting that some protein from SCAFs was taken up and possibly degraded by the recipient cells. However, in most cases, the L-HPG labeled proteome from the SCAFs persisted as large extracellular accumulations, that were still detectable two-three days after treatment. This demonstrates that through SCAF formation and subsequent rupture, the intracellular content of senescent cells can be deposited outside, onto neighboring cells.

The release of intracellular protein and organelles into the microenvironment can have diverse effects, depending on the content. To investigate the protein content that is released from SCAFs, we FACS isolated them at two different timepoints (days 5 and 10 after irradiation), and performed Mass Spectrometry (MS) analysis (Figure 5A). This identified the SCAF-associated proteome, revealing strong overlap in protein content among the replicates, and identifying 1376 proteins common to the four replicates (Figure 5B). Pathway analysis on these common proteins demonstrated a predicted interaction of the protein content with immune cell recruitment and activation, in particular neutrophils, myeloid cells and T-cells (Figure 5C). In addition, there was pronounced association with both NfKB and Wnt signaling pathways (Figure 5C). When we looked at KEGG pathway association, terms related to cell-cell adhesion appeared, including *adherens junction*, supporting our EM findings, and reinforcing the method of formation of the SCAFs (Figure 5D). Interestingly, there was a strong association of the protein content with disease, in particular neurodegenerative disease, including *Parkinson's disease*, *Amyotrophic lateral sclerosis, Huntington's and Alzheimer's disease*, all situations where senescence has previously been implicated.

When we looked at individual proteins, we detected most of the protein components of adherens junctions, including alpha- and beta-catenin, vinculin, vasp and others (Figure 5E). In addition, there were many cell surface proteins that have been associated with immune cell

recruitment and senescence including Calreticulin, CD44, CD47, and DPP4, a suggested marker of senescent cells (27) (Figure 5E). Importantly, we were able to validate our MS findings by immunostaining for many of these proteins on isolated SCAFs (Figure 5F).

It was also evident that many proteins known as damage-associated molecular patterns (DAMPs) are highly expressed in the SCAFs (Figure 5G). These include calreticulin, ferritin, multiple Histones, Heat Shock Proteins, Cathepsins and High Mobility group proteins, among others, findings which were also validated by immunostaining for individual examples on isolated SCAFs (Figure 5H). This strongly supports that a complex mixture of organelles, as well as intracellular and membrane-associated proteins are released through SCAF formation and rupture.

DAMPs play complex biological roles, influencing a variety of cell behaviors, including immune cell activation and recruitment, and cell migration and invasion linked to wound repair. We therefore sought to ask what effect SCAF exposure would have on cells. To address this, we performed RNA-sequencing on cells exposed to SCAFs. We isolated SCAFs from senescent cells and added them to proliferating IMR90 cells for 20 hours, before sequencing the treated cells (Figure 6A). In this scenario, we used inert resin beads that were FACS isolated as a negative control. Analyzing the RNA sequencing revealed that SCAF treatment resulted in 265 genes being significantly upregulated, and 316 genes downregulated (Figure 6B). Pathway analysis on upregulated differentially expressed genes (DEGs) supported a strong correlation with SCAFs promoting proliferation, migration and invasion, with GO biological process terms such as *wound healing*, *regulation* of *cell motility*, *cell population proliferation*, p*ositive regulation of cell migration*, and *cell adhesion* associating with the upregulated genes (Figure 6C). Analysis of KEGG associated terms revealed pathways associated with cancer, including *pathways in cancer*, *small cell lung cancer*, and *p53 signaling pathway*. Similar analysis on the downregulated genes further supported these changes, including GO biological process terms like *cell migration*, *cell motility, cell population proliferation* and *response to wounding* (Figure 6D). Supporting this association, genes such as MMP1, MMP14 and MMP16 were induced by SCAFs, while their potential substrates Collagens 1A1, 1A2, 3A1, 4A2, 5A1 and 5A2 were decreased.

To determine whether functional changes were supported by these associations, we examined cells exposed to SCAFs. As expected from the sequencing results, exposure of IMR90 fibroblasts to isolated SCAFs from senescent cells caused a significant increase in proliferation after twenty-four hours (Figure 6E). Similarly, in migration assays, cells exposed to SCAFs exhibited greater migration velocity (Figure 6F).

As there was such a strong association with cancer signaling, and given that SCAFs are also induced in senescent cancer cells, we also functionally investigated the effects of SCAF-exposure to cancer cells in culture. Here, we found that addition of SCAFs to liver cancer cells in culture also increased proliferation (Figure 6G). Furthermore, when we added SCAFs to cancer cells in 3D culture, within days, the SCAF-treated cells began to invade the gel, forming branches (Figure 6H, I). This supports our profiling and demonstrates that SCAFs can promote cell proliferation, migration and invasion in different contexts.

DISCUSSION

Here we describe a previously uncharacterized feature of senescent cells, cellular fragmentation. We identify that large pieces of senescent cells are broken off through cell-cell adhesion, and have termed these “senescent cell adhesion fragments” (SCAFs). We have identified SCAFs in every senescent cell type examined, including human and mouse cells, epithelia and fibroblasts. They are also detectable independently of the method used to induce senescence, including irradiation, oncogene expression and chemotherapeutic drugs, and importantly, we find SCAFs associated with senescent cells in vivo, in OIS in mouse hepatocytes. This raises an interesting possibility that SCAFs could help with identifying senescent cells in tissues. One of the main challenges with studying senescence is the lack of a universal marker (4). Senescence is usually identified in cells that activate a number of shared features, that together indicate the senescent state, but which individually may reflect a specific senescence-unrelated function. For example, p16 is often used as a marker of senescence. However, p16 expression alone is not sufficient to indicate senescence. SA-β-gal is another common marker for senescence, but can also label non-senescent cells such as macrophages (28). Our data supports that SCAFs might serve as another feature that can be used to identify senescent cells.

We uncovered that SCAFs form through adhesion of the senescent cell to their neighbors, which can be proliferating or senescent, and tearing of the fragment from the cell as they move apart. This raises a number of interesting questions about their genesis. Perhaps unexpectedly, senescent cells in culture were quite dynamic and active, and did not merely stay attached and motionless. There was constant movement and interaction with other cells. While it is known that cells constantly explore their environment, generating transient contacts with neighboring cells, why the senescent cells adhere so strongly to the other cells is unknown. We found multiple lines of evidence implicating adherens junctions, including their identification in EM and Mass Spec. We did not detect N- or E-cadherin in our MS analysis, but these might likely have been lost during the isolation process. Therefore, in this setting, it

appears that assembly of the AJ is functional, but the disassembly process might be impaired. AJs are constantly assembled and dissembled, which involves lysosomal degradation and turnover of some of the components (29,30). As lysosomal function is frequently impaired in senescent cells, this could suggest one reason for reinforced adhesion. Furthermore, it is known that AJ formation is reinforced by calcium (29,31). Interestingly, recent studies showed senescent cells have increased intracellular calcium, suggesting one other possible connection (32). Finally, SCAFs form by tearing of the cell membrane at sites away from the point of contact, suggesting also that there may be weaknesses in the membrane of senescent cells. However, it is intriguing that after generation, both the SCAF and the cell from which it formed, remain intact, suggesting that membrane repair mechanisms are active.

The identification of SCAFs raises intriguing questions about their nature and functions. Were SCAFs evolutionarily selected to exert specific functions, or are they a byproduct of a damaged and degenerating senescent state? Perhaps one informative hint here is the protein content of the SCAFs. Among the many proteins identified, the presence of DAMPs is notable. This diverse group of factors, also known as alarmins or danger signals, includes many cytosolic proteins, such as Heat Shock proteins, S100 family members, Annexins, histones, calreticulin, in addition to extracellular RNA and membrane lipids (25,33,34). When these become misplaced, and come to reside outside the cell, for example following necrosis, their presence serves as signals to activate the immune response, recruiting and stimulating activation of macrophages, neutrophils and other immune cells (25,35). Interestingly, some DAMPs have previously been linked with senescence. HMGB1 is a classical DAMP, that is also secreted by senescent cells as part of the SASP (26), while a recent proteomic analysis of the SASP also identified DAMPs in the conditioned media of senescent cells (7). The identification that SCAFs contain many DAMPs, and that they ultimately rupture and release their intracellular content onto the surface of neighboring cells, uncovers an additional way in which these proteins can be released by senescent cells, and a new way in which senescent cells communicate with their environment.

As to the functional role of SCAFs and their contents, again we can extrapolate based initially on their protein contents. Many of the proteins, including adherens junctions and DAMPs play critical roles in wound repair, stem cell function and activation of the immune system (31,35,36). Our pathway analysis on the SCAF protein content strongly supports activation of immune responses, including neutrophil and macrophages, the earliest responders to wounding. In addition, adding SCAFs to fibroblasts activates pathways associated with wound repair, proliferation, invasion and migration, features which we could functionally validate in cells in culture. As there is a strong association of senescent cells with stemness and wound

repair in various settings (11,37,38), this suggests that SCAFs may also play a positive role. It will be interesting to investigate if SCAFs are indeed generated by senescent cells in such beneficial settings, or if they are more related to damage-associated senescent cells.

However, DAMPs are most frequently linked to the process of inflammaging, a chronic sterile inflammation indicative of aged tissues, including a persistent activation of immune cells (25,34). This is thought to arise from the misplacement of self-molecules, including proteins, organelles and other classical DAMPs that are released from damaged or dead cells. Inflammaging is an active contributor to the aging process, and is a risk-factor for many age-related diseases (24,34). As senescent cells accumulate in aged tissues, and are detectable in higher numbers in many diseased tissues associated with aging, there is a strong correlation between senescence and inflammaging. However, how senescence contributes to inflammaging is unclear. As mentioned, some DAMPs are known SASP factors, such as HMGB1. Other SASP factors include cytokines that recruit and activate immune cells. The identification that SCAFs contain a wide variety of DAMPs makes yet another link that increased numbers of senescent cells in aged and damaged tissues could contribute to the inflammaging process.

Our data also suggests that the protein content of SCAFs is linked to many disease pathways, in particular neurodegeneration. Given the nature of the SCAFs, as large fragments of senescent cells, this association is perhaps expected, as senescence has been functionally implicated in a number of neurodegenerative diseases, including Alzheimer's and Parkinson's disease (18,20,39). However, as the SCAFs contain many proteins linked with these diseases, it will be interesting to study SCAF formation and functions specifically in these settings. Furthermore, it appears that the SCAFs undergo degeneration from the moment of formation, yet the timing of rupture seems variable. This would suggest that the proteins released by SCAF lysis may have undergone extensive modification or partial degeneration, before release. Additionally, as the release of "self-proteins" is strongly linked with auto-immune disease (24,25), it will be worthwhile to determine in situations of aging or damage if SCAF lysis might serve as an inducer of auto-antibodies. Finally, we find strong association with SCAFs and cancer. We have shown SCAFs are induced in situations of therapy-induced senescence, while addition of isolated SCAFs to fibroblasts activates pathways associated with cancer, including migration and invasion. Then, when added to liver cancer cells in culture, SCAFs promote proliferation, and induce invasion and migration in 3D. Together, this supports that the study of SCAF function in cancer is also warranted.

Overall, the identification of SCAFs uncovers yet another feature in the complex biology of senescence. While the precise functions of these structures remain to be unraveled, the data generated here can provide some hints. As the protein content of SCAFs, and the transcriptional readout of their effects on cells is strongly associated with immune cell recruitment, wound repair, invasion and migration, we speculate that SCAFs function as an additional mechanism to signal to and boost the immune response to sites where senescence is induced. As we have mostly studied SCAFs in situations without an active immune response, it will be interesting to see if SCAF formation is altered in the presence of immune cells. However, much like senescent cells themselves, which can have beneficial roles when induced in a timely, controlled manner, but become detrimental in chronic situation, increased SCAF formation associated with increased senescence burden will likely have detrimental effects associated with aging, cancer and other diseases.

MATERIALS AND METHODS

Cells

All cells were cultured at 37°C in 5% CO2. IMR90 were cultured in DMEM 41966 + 10% FBS + 100 U/ml penicillin-streptomycin. Huh-7 cells were cultured in RPMI 1640 w/10mM HEPES + 10% FCS + 2.5g/L Glucose + 1mM Sodium Pyruvate + 50 μM β-mercaptoethanol + 40 μg /mL gentamycine. All cell lines were routinely tested for the presence of mycoplasma.

Cell viral transduction

Transduction with retroviral vector was used to generate IMR90 and Huh-7 cells stably expressing the green fluorescent protein (GFP). Retrovirus was produced by transiently transfecting the Phoenix packaging cell line (G. Nolan, Stanford University, Stanford, CA) with MSCV vector containing GFP coding sequence. Cells were infected with virus for 24 h, drug-selected in 1 µg/mL puromycin for 48 h, and subsequently tested for presence of replicatively competent virus.

To generate IMR90 cells stably expressing GFP and 4-hydroxy tamoxifen inducible ER:ras fusion protein, IMR90 cells stably expressing GFP were transduced with a retroviral vector encoding the ER:ras protein (Narita, https://www.addgene.org/67844/). Cells were infected with virus for 24 h, selected for 7 days in 500 µg/mL G418 and subsequently tested for presence of replicatively competent virus.

Induction of senescence

For ionizing radiation induced senescence, cells were exposed to a dose of 10 Gy of X-rays using CellRad Precision X-ray irradiator. The device was set to 130 kV and 5 mA at the tray position at one, leading to dose rate of 0.92 Gy/min.

For oncogene induced senescence, cells expressing the ER:ras protein were exposed to 500nM of 4-hydroxy tamoxifen for the full duration of the experiment.

For therapy induced senescence, cells were treated with 200 nM doxorubicin for 24 hours. Afterwards, the culture was washed and cultured in regular medium.

Correlative light and electron microscopy (CLEM)

Fragmenting cells were cultured on laser micro-patterned Aclar supports (1,2). Using a spinning disc confocal microscope (Leica) a time-lapse acquisition was performed, followed by immediate fixation of cells and fragments using 2.5% glutaraldehyde and 2.5% formaldehyde in 0.1M cacodylate buffer for 1 hour at 4°C. After washing, the samples were post-fixed for 1 hour in 1% osmium tetroxide [OsO4] reduced by 0.4% potassium hexacyanoferrate (III) [K3Fe(CN)6] in H2O at +4°C. After extensive rinses in distilled water, samples were then stained by 1% uranyl acetate for 1 hour at +4°C, and rinsed in water. Samples were dehydrated with increasing concentrations of ethanol (25%, 50%, 70%, 90% and 3x100%), and embedded with a graded series of epoxy resin. Samples were finally polymerized at 60°C for 48 hours. Ultrathin serial sections (60nm) were picked up on 1% pioloform coated copper slot grids and observed with a Philips CM12 TEM electron microscope (Philips, FEI Electron Optics, Eindhoven, Netherlands) operated at 80kV equipped with an Orius 1000 CDD camera (Gatan, Pleasanton, USA).

Fluorescence-Activated Cell Sorting (FACS) isolation

FACS was used to isolate senescent cells and SCAFs. Two million IMR90 cells stably expressing GFP and seeded into a p15 petri dish were X-ray irradiated and subsequently cultured for 5-10 days. Before sorting, cells were washed twice with PBS after which 4.5 ml of Accutase (STEMCELL technologies) was added, to dissociate cells and SCAFs and the dish was placed in an incubator. After five minutes cells were gently resuspended using a 5 mL serological pipette and incubated for 5 more minutes. Afterwards, 5.5 mL of 2% FBS in PBS was added and cells were again gently resuspended using 10 mL serological pipette. Then, cells were centrifuged at 290 rcf for 4 minutes. Supernatant was discarded and the pellet resuspended in 3 mL of Pre-Sort Buffer (BD biosciences). Gating was set as in Fig. 4A and

fragments or cells were sorted at RT and collected into 1.5 mL Eppendorf tubes with 350 µl of standard media.

Cytospin
FACS sorted cells or fragments were fixed in 4% PFA for 15 minutes at RT and then washed 3x by PBS. Suspension of 150 µL was added into a cytospin funnel mounted on poly-lysine coated microscope slide and centrifuged at 1000 RPM for 5 minutes. Afterwards, the sample was fixed in 4% PFA for 15 minutes at RT, to attach the sample to the slide surface.

Immunofluorescence
Cells/fragments for immunofluorescence were cytospun (see above) or fixed in 4% PFA for 15 minutes at RT followed by 3x PBS wash. Next, the sample was permeabilized for 10 min in PBS + 0.1% Triton-X and washed 3x by PBS. Blocking was done using PBS + 10% goat serum + 0.1% Tween for 1 hour at RT. Primary and secondary antibodies were diluted in PBS +1% goat serum + 0.1% Tween. After blocking, sample was incubated with primary antibody for 1 hour at RT, followed by 3x PBS wash. Then, secondary antibody was added for 1h at RT followed by 3x PBS wash. Subsequently, nuclei were counterstained using DAPI 1 µg/ml for 10 minutes at RT, and actin filaments were counterstained using Phalloidin-AF568 (ThermoFischer) 165 nM. Sample was then washed 3x by PBS and mounted using Fluoromount-G (ThermoFischer).
For immunofluorescent imaging, livers were fixed with 10% neutral buffered formalin for 24 hrs at 4°C and stored in 70% EtOH until further processing. Fixed liver tissues were washed in PBS and sectioned at 100 µm using vibratome. Sections were permeabilized using PBS + 0.5% Triton-X at 4°C overnight. Blocking was done at 4°C for 24 hours in PBS + 10% goat serum + 0.1% Triton-X and primary and secondary antibodies were dissolved in PBS+1% goat serum +0.01% Triton-X. Following blocking, sections were incubated in primary antibody for 24 hours at 4°C, followed by 3x 2-hour wash at 4°C in PBS + 0.01% Triton-X and 24-hour incubation at 4°C with secondary antibody. Afterwards, sections were stained with DAPI 1 µg/ml for 1 hour at 4°C and washed in PBS + 0.01% Triton-X for 3x 2-hours at 4°C. Sections were then mounted on a microscope slide and cleared by serial treatment with 60%, 80% and 87% glycerol for 2 hours per step. Afterwards, samples were mounted in 87% glycerol.

Primary antibodies were used at following concentrations: anti-GFP (1:1000, Abcam, ab13970), anti-DPP4 (1:300, Abcam, ab28340), anti-CTNNB1 (1:500, Abcam, ab16051), anti-CD44 (1:1000, ab15710), anti-CD47 (1:1000, BioXcell, MIAP410), anti-ANXA2 (1:500, BD biosciences, 610069), anti-CD166 (1:500, Abcam, ab109215), anti-Histone H4 (1:300, Abcam, ab10158), anti-HSPD1 (1:300, In-House produced, clone: 4MTE-2H7), anti-CALR (1:500, Abcam, ab2907), anti-S100A9 (1:1000, Abcam, ab92507). Alexa-conjugated secondary antibodies were used in the dilution of 1:1000 – 1:2000.

L-HPG whole proteome labeling
Proliferating GFP labelled IMR90 cells were treated with 200 µM L-homopropargylglycine (L-HPG) in standard medium. Afterwards, cells were seeded for fragment isolation and X-ray irradiated to induce senescence, while continuously being treated with 200 µM L-HPG. After FACS isolation of SCAFs, 60 000 SCAFs were seeded onto proliferating GFP negative IMR90 cells. After 48 hours, cells were directly fixed by adding equal volume of 8% PFA on top of cell culture medium and incubating for 15 minutes at RT. Staining protocol is the same as for EDU proliferation assay followed by GFP immunostaining (see below and above respectively).

EDU proliferation assay
Cells were incubated with 20 µM of EDU in standard medium for 2 hours. Subsequently, cells were 1x washed with PBS and fixed for 15 minutes in 4% PFA at RT. After fixation, samples were incubated with 100 mM Tris for 5 minutes and permeabilized with PBS + 0.1% Triton-X for 10 minutes. Following 3x wash with PBS, cells were stained using Click-staining solution containing Sulfo-Cy3-Azide for 30 minutes at RT. Subsequently, samples were washed 3x with

PBS, stained with DAPI 1 µg/ml for 10 minutes at RT, washed 3x with PBS and mounted using Fluoromount.

Time-lapse and confocal microscopy

For acquisition of in-vitro senescent cells and senescent hepatocytes in liver sections, Leica CSU-W1 spinning disk, 63× objective, oil immersion was used with Z step of 0.3 µm.
For confocal images of fragmenting cells Leica SP5 inverted confocal microscope was used with 63x objective, oil immersion.
For live-cell imaging cells were seeded in a 30 mm diameter glass-bottom dish. For acquisition, Zeiss Axio Observer Z1 microscope with 20x dry objective was used. Cells were treated with 30 000 SCAFs and were placed into a humid heated chamber with 5% CO2 and 80% humidity in the microscope. Four positions were selected for each condition and pictures were taken every 5 minutes for 8 hours.

Mass spectrometry analysis of SCAF proteome

After FACS isolation, GFP positive SCAFs were centrifuged at 400g for 5 minutes at room temperature and the pellet was snap-frozen in liquid nitrogen. Proteins were then precipitated using trichloroacetic acid, followed by acetone wash. Mass spectrometry was performed on Orbitrap Elite using the Top20CIDr method, with 2 hours run and 3 repetitions. Results were analyzed using Proteome Discoverer 1.4 and compared with homo sapiens_181015 database. Thresholds of 1% FDR and minimum of 2 peptides per protein were applied. Pathway analysis was performed using gProfiler (https://biit.cs.ut.ee/gprofiler/gost). Gene Ontology Databases and KEGG biological pathway database were considered. Adjusted p-value of <0.05 was used as a threshold to select the significant enrichment.

RNA sequencing of SCAF treated cells

Proliferating GFP negative IMR90 cells were treated with 300 000 SCAFs or inert beads for 20 hours under normal culture conditions. Four independent biological replicates per condition were generated. Cells were washed 1x with PBS and lysed in 350 µl of Guanidine thiocyanate-based lysis buffer (LBP lysis buffer, Macherey-Nagel NucleoSpin RNA plus isolation kit, Ref. 740984), RNA was isolated and sent to the GenomEast platform at Institut de Génétique et de Biologie Moléculaire et Cellulaire (IGBMC). Library was prepared using TruSeq Stranded mRNA Library preparation (Illumina). Sequencing was performed with HiSeq 4000 technology (Illumina) on single-end 50bp length reads. Reads were pre- processed to remove low quality and short (<40bp) reads using cutadapt v1.10. Remaining reads were mapped onto the hg38 assembly of Homo sapiens genome using STAR version 2.5.3a. Gene expression quantification was performed from uniquely aligned reads using htseq-count version 0.6.1p1, with annotations from Ensembl version 98 and “union” mode. Read counts have been normalized across samples with the median-of-ratios method proposed by Anders and Huber, to make these counts comparable between samples. Differential gene expression analysis was performed using Wald test, as proposed by Love et al. and implemented in the Bioconductor package DESeq2 version 1.16.1. P-values were adjusted for multiple testing using the Benjamini and Hochberg method. Genes with an adjusted p-value <0.05 were considered significantly differentially expressed. Pathway analysis was performed using gProfiler (https://biit.cs.ut.ee/gprofiler/gost). Gene Ontology Databases and KEGG biological pathway database were considered. Adjusted p-value of <0.05 was used as a threshold to select the significant enrichment.

Cell motility assay

Proliferating IMR90 cells were seeded in a 4 chamber 30 mm diameter glass-bottom dish (IBL, Ref 220.120.022) with 8000 cells per chamber. For acquisition, Zeiss Axio Observer Z1 microscope with 20x dry objective was used. Cells were treated with Hoechst 33342 0.5 µg/ml, 30 000 SCAFs or inert beads and were placed into a humid heated chamber with 5% CO2 and 80% humidity in the microscope. Four positions were selected for each condition and pictures

were taken for 8 hours every 5 minutes. Cell nuclei were automatically detected using StarDist and subsequently tracked using the TrackMate ImageJ modules.

Focus formation assay

Huh-7 cells were seeded into 6 well plates in two different densities – 2000 cells and 4000 cells per well. At 24 and 48 hours after seeding, cells were treated either by normal medium or by 60 000 SCAFs isolated from senescent IMR90 cells expressing GFP. After 10 days, cells were fixed in 4% PFA at RT for 15 minutes and washed with PBS. Subsequently, cells were stained with crystal violet using a standard protocol.

Spheroid Matrigel-invasion assay

To generate spheroids derived from Huh-7 cells, 40 000 cells were seeded into Ultra-low adhesion 96 well plates (Corning). After 48 hours, formed spheroids were treated either with standard medium or 30 000 SCAFs. Plate was then centrifuged at 300g for 5 minutes. Supernatant was aspirated and spheroids were embedded in Matrigel +10% rat tail collagen. Spheroids were imaged daily using a 5x dry objective. Six technical replicates were performed in each independent experiment. The day of first visible outgrowth was noted and the average per condition and experiment plotted.

Statistical analysis

Unless specifically stated, results are presented as mean ± SEM. Statistical significance was determined by the two-tailed unpaired Student's t-test.

REFERENCES

1. Rhinn M, Ritschka B, Keyes WM. Cellular senescence in development, regeneration and disease. Dev. 2019;146(20).
2. Muñoz-Espín D, Serrano M. Cellular senescence: From physiology to pathology. Nat Rev Mol Cell Biol. 2014;15(7):482–96.
3. Childs BG, Gluscevic M, Baker DJ, Laberge RM, Marquess D, Dananberg J, et al. Senescent cells: An emerging target for diseases of ageing. Nat Rev Drug Discov. 2017;16(10):718–35.
4. Gorgoulis V, Adams PD, Alimonti A, Bennett DC, Bischof O, Bishop C, et al. Cellular Senescence: Defining a Path Forward. Cell. 2019;179(4):813–27.
5. Schmitt CA, Wang B, Demaria M. Senescence and cancer — role and therapeutic opportunities. Vol. 19, Nature Reviews Clinical Oncology. Springer US; 2022. p. 619–36.
6. Coppé JP, Desprez PY, Krtolica A, Campisi J. The senescence-associated secretory phenotype: The dark side of tumor suppression. Annu Rev Pathol Mech Dis. 2010;5:99–118.
7. Basisty N, Kale A, Jeon OH, Kuehnemann C, Payne T, Rao C, et al. A proteomic atlas of senescence-associated secretomes for aging biomarker development. PLoS Biol. 2020;18(1):e3000599.
8. Birch J, Gil J. Senescence and the SASP: Many therapeutic avenues. Genes Dev. 2020;34(23–24):1565–76.
9. Storer M, Mas A, Robert-Moreno A, Pecoraro M, Ortells MC, Di Giacomo V, et al. Senescence is a developmental mechanism that contributes to embryonic growth and patterning. Cell. 2013 Nov 21;155(5).
10. Muñoz-Espín D, Cañamero M, Maraver A, Gómez-López G, Contreras J, Murillo-Cuesta S, et al. Programmed cell senescence during mammalian embryonic development. Cell. 2013;155(5):1104.
11. Demaria M, Ohtani N, Youssef SA, Rodier F, Toussaint W, Mitchell JR, et al. An essential role for senescent cells in optimal wound healing through secretion of PDGF-AA. Dev Cell. 2014;31(6):722–33.
12. Mosteiro L, Pantoja C, Alcazar N, Marión RM, Chondronasiou D, Rovira M, et al. Tissue damage and senescence provide critical signals for cellular reprogramming in vivo. Science (80-). 2016;354(6315).
13. Ritschka B, Storer M, Mas A, Heinzmann F, Ortells MC, Morton JP, et al. The senescence-associated secretory phenotype induces cellular plasticity and tissue regeneration. Genes Dev. 2017;1–12.
14. Kang TW, Yevsa T, Woller N, Hoenicke L, Wuestefeld T, Dauch D, et al. Senescence surveillance of pre-malignant hepatocytes limits liver cancer development. Nature. 2011;479(7374):547–51.
15. Binet F, Cagnone G, Crespo-Garcia S, Hata M, Neault M, Dejda A, et al. Neutrophil extracellular traps target senescent vasculature for tissue remodeling in retinopathy. Science (80-). 2020;369(6506).
16. Baker DJ, Childs BG, Durik M, Wijers ME, Sieben CJ, Zhong J, et al. Naturally occurring p16 Ink4a-positive cells shorten healthy lifespan. Nature. 2016;530(7589):184–9.
17. Xu M, Pirtskhalava T, Farr JN, Weigand BM, Palmer AK, Weivoda MM, et al. Senolytics improve physical function and increase lifespan in old age. Nat Med. 2018;24(8):1246–56.
18. Bussian TJ, Aziz A, Meyer CF, Swenson BL, van Deursen JM, Baker DJ. Clearance of senescent glial cells prevents tau-dependent pathology and cognitive decline. Nature. 2018;562(7728):578–82.
19. Schafer MJ, White TA, Iijima K, Haak AJ, Ligresti G, Atkinson EJ, et al. Cellular senescence mediates fibrotic pulmonary disease. Nat Commun. 2017;8.
20. Chinta SJ, Woods G, Demaria M, Rane A, Zou Y, McQuade A, et al. Cellular Senescence Is Induced by the Environmental Neurotoxin Paraquat and Contributes to

Neuropathology Linked to Parkinson's Disease. Cell Rep. 2018;22(4):930–40.
21. Demaria M, Leary MNO, Chang J, Shao L, Liu S, Koenig K, et al. Cellular senescence promotes adverse effects of chemotherapy and cancer relapse. 2018;7(2):165–76.
22. Niedernhofer LJ, Robbins PD. Senotherapeutics for healthy ageing. Nat Rev Drug Discov. 2018;17(5):377.
23. Sousa-Victor P, Gutarra S, García-Prat L, Rodriguez-Ubreva J, Ortet L, Ruiz-Bonilla V, et al. Geriatric muscle stem cells switch reversible quiescence into senescence. Nature. 2014;506(7488):316–21.
24. Furman D, Campisi J, Verdin E, Carrera-Bastos P, Targ S, Franceschi C, et al. Chronic inflammation in the etiology of disease across the life span. Nat Med. 2019;25(12):1822–32.
25. Franceschi C, Garagnani P, Vitale G, Capri M, Salvioli S. Inflammaging and 'Garb-aging.' Trends Endocrinol Metab. 2017;28(3):199–212.
26. Davalos AR, Kawahara M, Malhotra GK, Schaum N, Huang J, Ved U, et al. p53-dependent release of Alarmin HMGB1 is a central mediator of senescent phenotypes. J Cell Biol. 2013;201(4):613–29.
27. Kim KM, Noh JH, Bodogai M, Martindale JL, Yang X, Indig FE, et al. Identification of senescent cell surface targetable protein DPP4. Genes Dev. 2017;31(15):1529–34.
28. Hall BM, Balan V, Gleiberman AS, Strom E, Krasnov P, Virtuoso LP, et al. p16(Ink4a) and senescence-associated β-galactosidase can be induced in macrophages as part of a reversible response to physiological stimuli. Aging (Albany NY). 2017;9(8):1867–84.
29. Green KJ, Getsios S, Troyanovsky S, Godsel LM. Intercellular junction assembly, dynamics, and homeostasis. Vol. 2, Cold Spring Harbor perspectives in biology. 2010. p. 1–23.
30. Palacios F, Tushir JS, Fujita Y, D'Souza-Schorey C. Lysosomal Targeting of E-Cadherin: a Unique Mechanism for the Down-Regulation of Cell-Cell Adhesion during Epithelial to Mesenchymal Transitions. Mol Cell Biol. 2005;25(1):389–402.
31. Biswas R, Banerjee A, Lembo S, Zhao Z, Lakshmanan V, Lim R, et al. Mechanical instability of adherens junctions overrides intrinsic quiescence of hair follicle stem cells. Dev Cell. 2021;56(6):761-780.e7.
32. Wiel C, Lallet-Daher H, Gitenay D, Gras B, Le Calvé B, Augert A, et al. Endoplasmic reticulum calcium release through ITPR2 channels leads to mitochondrial calcium accumulation and senescence. Nat Commun. 2014;5(May).
33. Huang J, Xie Y, Sun X, Zeh HJ, Kang R, Lotze MT, et al. DAMPs, ageing, and cancer: The "DAMP Hypothesis." Ageing Res Rev. 2015;24:3–16.
34. Franceschi C, Campisi J. Chronic inflammation (Inflammaging) and its potential contribution to age-associated diseases. Journals Gerontol - Ser A Biol Sci Med Sci. 2014;69:S4–9.
35. Hernandez C, Huebener P, Schwabe RF. Damage-associated molecular patterns in cancer: A double-edged sword. Oncogene. 2016;35(46):5931–41.
36. Vénéreau E, Ceriotti C, Bianchi ME. DAMPs from cell death to new life. Front Immunol. 2015;6(AUG):1–11.
37. Ritschka B, Storer M, Mas A, Heinzmann F, Ortells MC, Morton JP, et al. The senescence-associated secretory phenotype induces cellular plasticity and tissue regeneration. Genes Dev. 2017;31(2):172–83.
38. Mosteiro L, Pantoja C, de Martino A, Serrano M. Senescence promotes in vivo reprogramming through p16 INK4a and IL-6. Aging Cell. 2018;17(2).
39. Musi N, Valentine JM, Sickora KR, Baeuerle E, Thompson CS, Shen Q, et al. Tau protein aggregation is associated with cellular senescence in the brain. Aging Cell. 2018;17(6):e12840.

FIGURE LEGENDS

Figure 1. Cells undergoing senescence form cell-cell adhesion dependent fragments.

(A) Experimental design of live cell imaging of individual GFP-labelled cells undergoing senescence.

(B) GFP, phase contrast (PH) and DAPI images of cells diluted as per the scheme in A, on day 5 after plating. Arrowheads indicate GFP containing cellular fragments in the cultures with senescent cells (Scale bar = 80 μm)

(C) Confocal image of senescent cell (green) diluted in GFP-negative cells, shows GFP fragments adhere to the membrane of adjacent cells in Sen-Sen condition. (Scale bar = 80 μm)

(D) Timelapse imaging of GFP senescent cells diluted in GFP-negative proliferating cells. Asterisk labels adhesion point between cells. Arrowhead labels senescent fragment formation (Scale bar = 80 μm)

(E) Quantification of fragments per cell at different time-points after senescence induction, in each culture condition. (Data are mean ± SEM of 3-5 biological replicates. Points indicate the mean of a single replicate.)

(F) Confocal micrographs of 4 different regions of interest (ROI) reveal the size and shape of senescent fragments. Top row shows anti-GFP immunostaining (green). Bottom row shows composites of chromatin (DAPI - blue) and actin (phalloidin – red) staining and anti-GFP immunostaining (green). (Scale bar = 40 μm.)

(G) Measurement of major axis length of fragments in cell-dilution cultures. (Red line indicates the mean of major axis length of all fragments, n=2327. Measurements were acquired from 3 biological replicates.)

(H) Experimental design of live cell imaging of individual GFP-labelled senescent cells. GFP, phase contrast (PH) and DAPI images of individually plated cells (Scale bar = 80 μm). Graph shows quantification of number of fragments per cell (salmon bars show the same results as in E for reference).

(I) Images of cell-dilution strategy using oncogene induced senescence (OIS) in human primary lung fibroblasts (IMR90) and irradiation- (IIS) and therapy- (TIS) induced senescence in human hepatocyte-derived carcinoma cell line (Huh7). (Scale bar = 80 μm, GFP, green; DAPI, blue)

Figure 2. SCAFs are present in oncogene-induced senescent mouse hepatocytes in vivo.

(A) Hematoxylin Eosin (H&E), SA-B-gal staining and GFP immunostaining were performed on liver sections 6 days after hydrodynamic tail-vein mediated delivery of active $Nras^{G12V}$, or inactive $Nras^{G12V/D38A}$ containing GFP coding sequences.

(B) Maximum Z projection confocal images of control ($Nras^{G12V/D38A}$) and senescent ($Nras^{G12V}$) liver hepatocytes expressing GFP. (GFP, green; DAPI, blue). Insets i and ii indicate regions of the image used for 3D rendering in the IMARIS software. (Scale bar = 80 μm)

(C) IMARIS rendering of control hepatocytes ($Nras^{G12V/D38A}$). (Scale bar = 20 μm)

(D) IMARIS rendering of senescent hepatocytes ($Nras^{G12V}$). White arrowheads indicate fragments not connected to senescent cell. (i scale bar = 10 μm, ii scale bar = 8 μm.)

Figure 3. SCAFs are large membrane bound bodies containing cytoplasm and organelles.

(A) Brightfield and GFP-image of live-cell microscopy of GFP-senescent cell dilution model. Inset indicates the region of interest for subsequent transmission electron microscopy (TEM).

(B) Magnified view of inset in A. Numbers indicate individual SCAFs later imaged by TEM.

(C) TEM image of the region of interest shown in B. Four GFP positive SCAFs are indicated. (Scale bar = 1 μm.)

(D) Higher magnification of GFP positive SCAFs 1-4 from C. (AJ, adherens junction: SER, smooth endoplasmic reticulum: M, mitochondria: LD, lipid droplet: RB, residual body: AP, autophagosome: R, ribosomes. Scale bar = 1 μm.)
(E) Additional SCAF showing adherens junction (AJ, adherens junction: RB, residual body, AP, autophagosome: M, mitochondria. Scale bar = 1 μm.)

Figure 4. SCAFs maintain their integrity for a limited time after which they rupture, release their cytoplasmic content and form cellular debris.
(A) Experimental design and gating of fluorescence-activated cell sorting (FACS) of intact, GFP positive senescing cells and SCAFs.
(B) Cytospin and immunostaining of senescent cells and SCAFs for GFP (green) with DAPI staining of DNA. (Scale bar = 80 μm)
(C) Image of living GFP positive (green) SCAFs isolated by FACS and seeded on top of proliferating GPF-negative IMR90 cells. (Scale bar = 80 μm)
(D) Representative images of GFP positive (green) SCAFs at different times (Days0-3) after seeding on proliferating GPF negative IMR90 cells. Arrowheads indicate residual GFP positive SCAFs surrounded by GFP negative cellular debris. (Scale bar = 80 μm)
(E) Timeframe images of GFP positive (green) SCAF rupture and debris generation. Arrowheads indicate SCAFs at different time-points. (Scale bar = 10 μm)
(F) Brightfield imaging at days (D) 1 and 3 after adding increasing number of SCAFs to culture generating increased cell debris (arrowheads). (Scale bar = 80 μm)
(G) Fluorescence microscopy for GFP positive SCAFs (green) and L-homopropargyl glycine (L-HPG) (red), stained with DAPI (blue) (Scale bar = 80 μm)

Figure 5. SCAFs contain proteins associated with innate immune processes, age-related diseases and contain Damage Associated Molecular Patterns (DAMPs).
(A) Experimental design of Mass Spectrometry (MS) analysis of the protein content of isolated SCAFs.
(B) Overlap of proteins identified in SCAFs by MS. (S1, sample 1; S2, sample 2; D5, day 5; D10, day 10).
(C) Bioinformatic analysis of SCAF proteome using gProfiler (GO Biological process) reveals strong association with immune-related processes and signaling.
(D) Bioinformatic analysis of SCAF proteome using gProfiler (KEGG pathway) reveals strong association with multiple age-related degenerative diseases.
(E) Tables indicating protein components of adherens junction complexes and representative cell surface proteins detected in SCAF-proteome.
(F) Immunofluorescence for representative surface marker proteins in isolated SCAFs. (Scale bar = 80 μm)
(G) Table listing DAMP proteins detected in SCAF-proteome.
(H) Immunofluorescence for selected DAMP proteins in isolated SCAFs. (Scale bar = 80 μm)

Figure 6. SCAFs promote proliferation, cell migration, and invasion of cancer cells.
(A) Experimental design of RNA sequencing analysis of primary human fibroblast (IMR90) after 20 hours of SCAF exposure.
(B) Volcano plot of differentially expressed genes between IMR90 cells treated with SCAFs compared to control cells treated with inert beads of similar size.
(C) Bioinformatic analysis of significantly upregulated genes after SCAF-exposure using gProfiler. GO Biological process and KEGG pathway terms are shown.
(D) Bioinformatic analysis of significantly downregulated genes after SCAF-exposure using gProfiler. GO Biological process and KEGG pathway terms are shown.

(E) EDU incorporation assay at different time points (D, days) after SCAF-exposure in IMR90 fibroblasts. (Data are mean ± SEM of proliferation relative to control cells in 4 biological replicates. Points indicate the value of a single replicate. * - $p<0.05$, two-sided T-test.)
(F) Cell motility measurement after SCAF-exposure in IMR90 fibroblasts, relative to untreated and inert bead treated controls. (Data are mean ± SEM of the median velocity in 5 biological replicates. Points indicate the median velocity of a single replicate. * - $p<0.05$, paired T-test.)
(G) Focus formation assay of human hepatocyte-derived carcinoma cell line (Huh-7) treated with SCAFs or medium on D0 and D2.
(H) Huh-7 spheroid Matrigel-invasion assay after SCAFs or medium treatment.
(I) Quantification of earliest observed invasion of Matrigel by Huh-7 derived spheroids from H. (Data are mean ± SEM of the mean first day of observed outgrowth in 3 biological replicates (Each consisting of 6 technical replicates). Points indicate the mean of a single biological replicate. *** - $p<0.005$, two-sided T-test.)

Supplementary Figure 1. The dynamics of senescence features in irradiation-induced senescence.
(A) Time-course of the expression of $p21^{CIP1}$ after senescence induction in IMR90 cells.
(B) Time-course of the expression of $p16^{INK4A}$ after senescence induction in IMR90 cells.
(A) Time-course of SA-B-gal positivity after senescence induction in IMR90 cells.

Supplementary Figure 2. Average major-axis length of FACS-isolated senescent cells and SCAFs.

Figure 1.

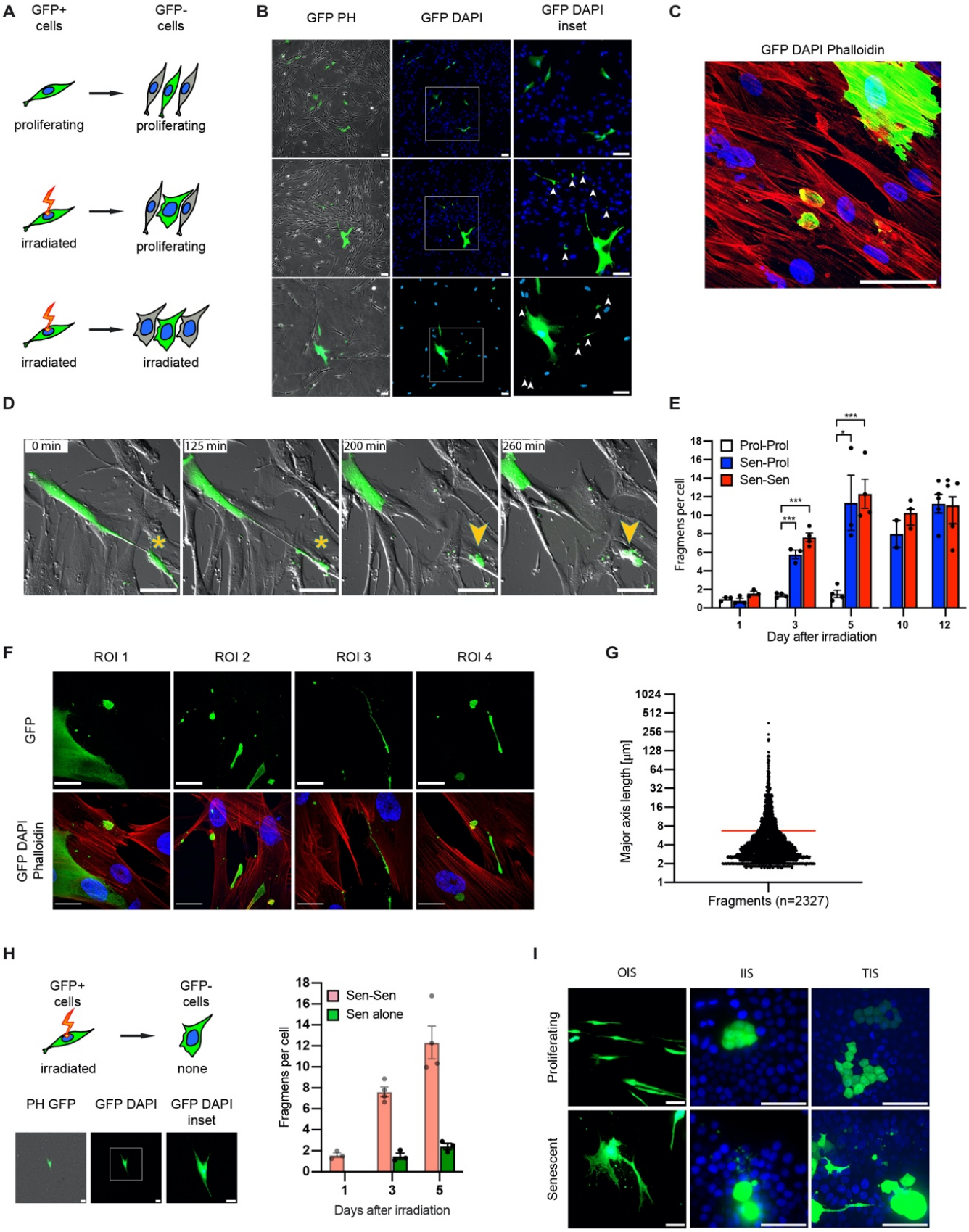
A
GFP+ cells
GFP- cells
proliferating
proliferating
irradiated
proliferating
irradiated
irradiated
B
GFP PH
GFP DAPI
GFP DAPI inset
C
GFP DAPI Phalloidin
D
0 min
125 min
200 min
260 min
E
Prol-Prol
Sen-Prol
Sen-Sen
Fragmens per cell
Day after irradiation
F
ROI 1
ROI 2
ROI 3
ROI 4
GFP
GFP DAPI Phalloidin
G
Major axis length [µm]
Fragments (n=2327)
H
GFP+ cells
GFP- cells
irradiated
none
PH GFP
GFP DAPI
GFP DAPI inset
Sen-Sen
Sen alone
Fragmens per cell
Days after irradiation
I
OIS
IIS
TIS
Proliferating
Senescent

Figure 2.

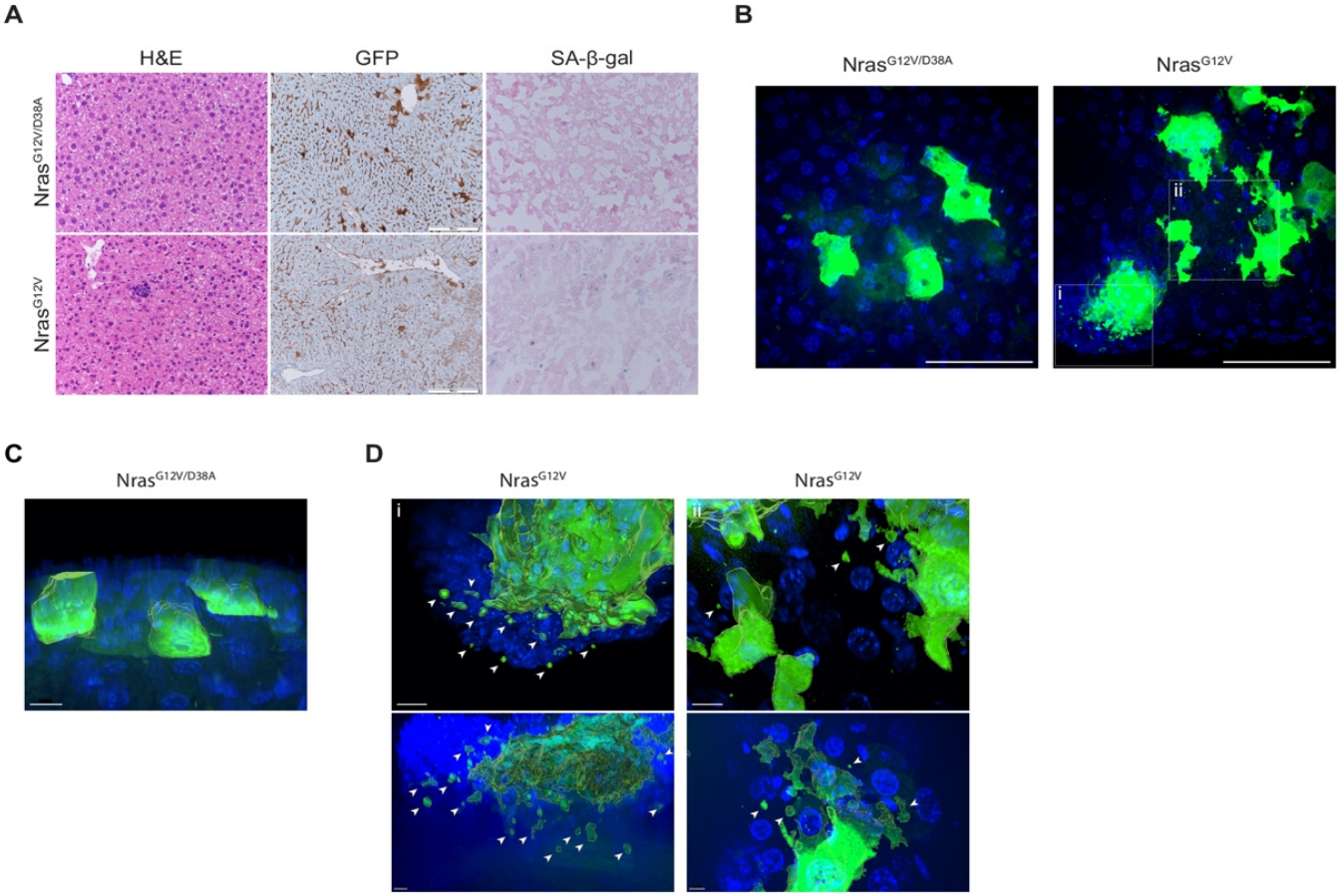
A
H&E
GFP
SA-β-gal
NrasG12V/D38A
NrasG12V
B
NrasG12V/D38A
NrasG12V
i
ii
C
NrasG12V/D38A
D
NrasG12V
NrasG12V
i
ii

Figure 3.

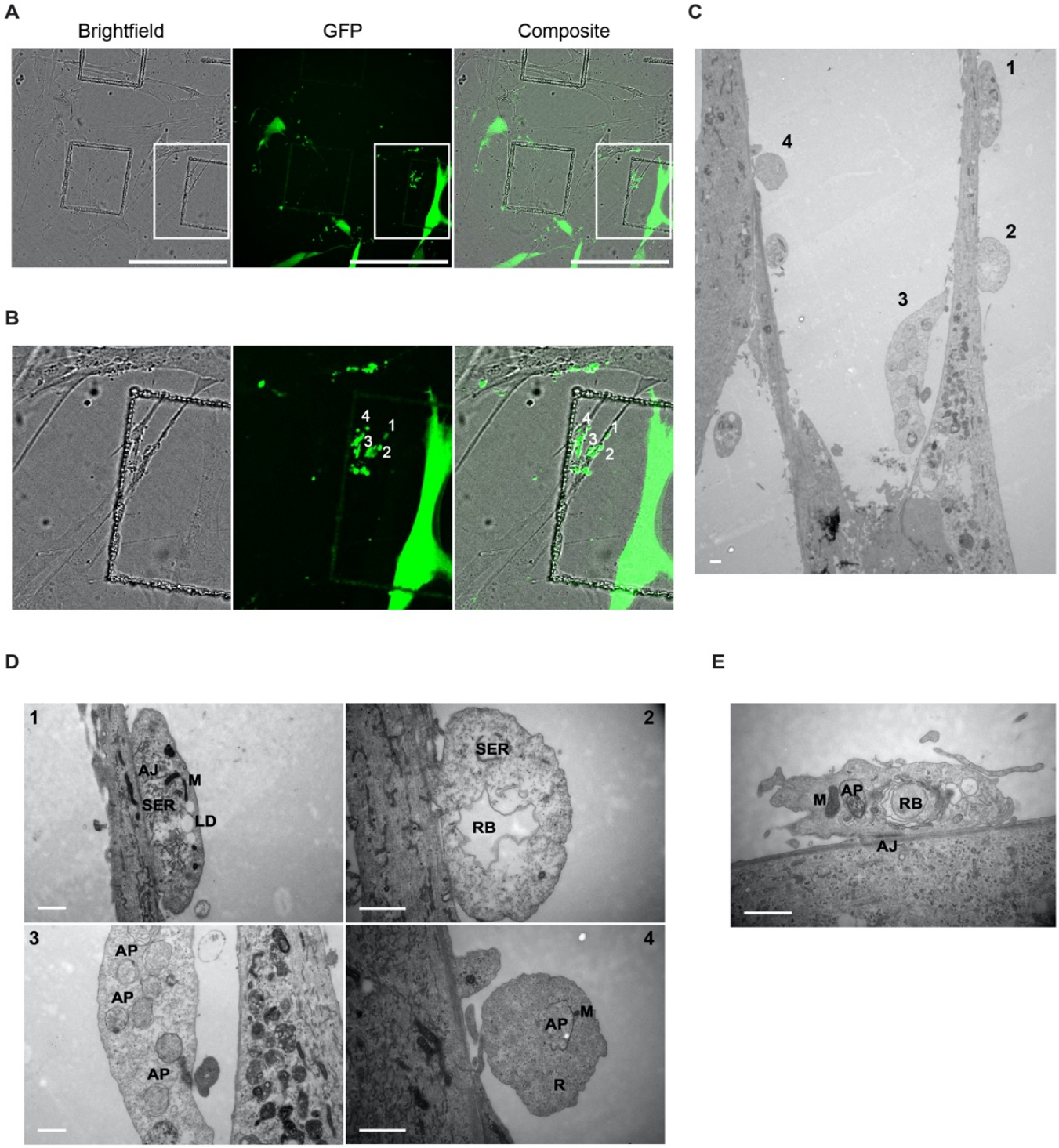
A
Brightfield
GFP
Composite
B
4
1
3
2
C
1
4
2
3
D
1
AJ
M
SER
LD
2
SER
RB
3
AP
AP
AP
4
M
AP
R
E
M
AP
RB
AJ

Figure 4.

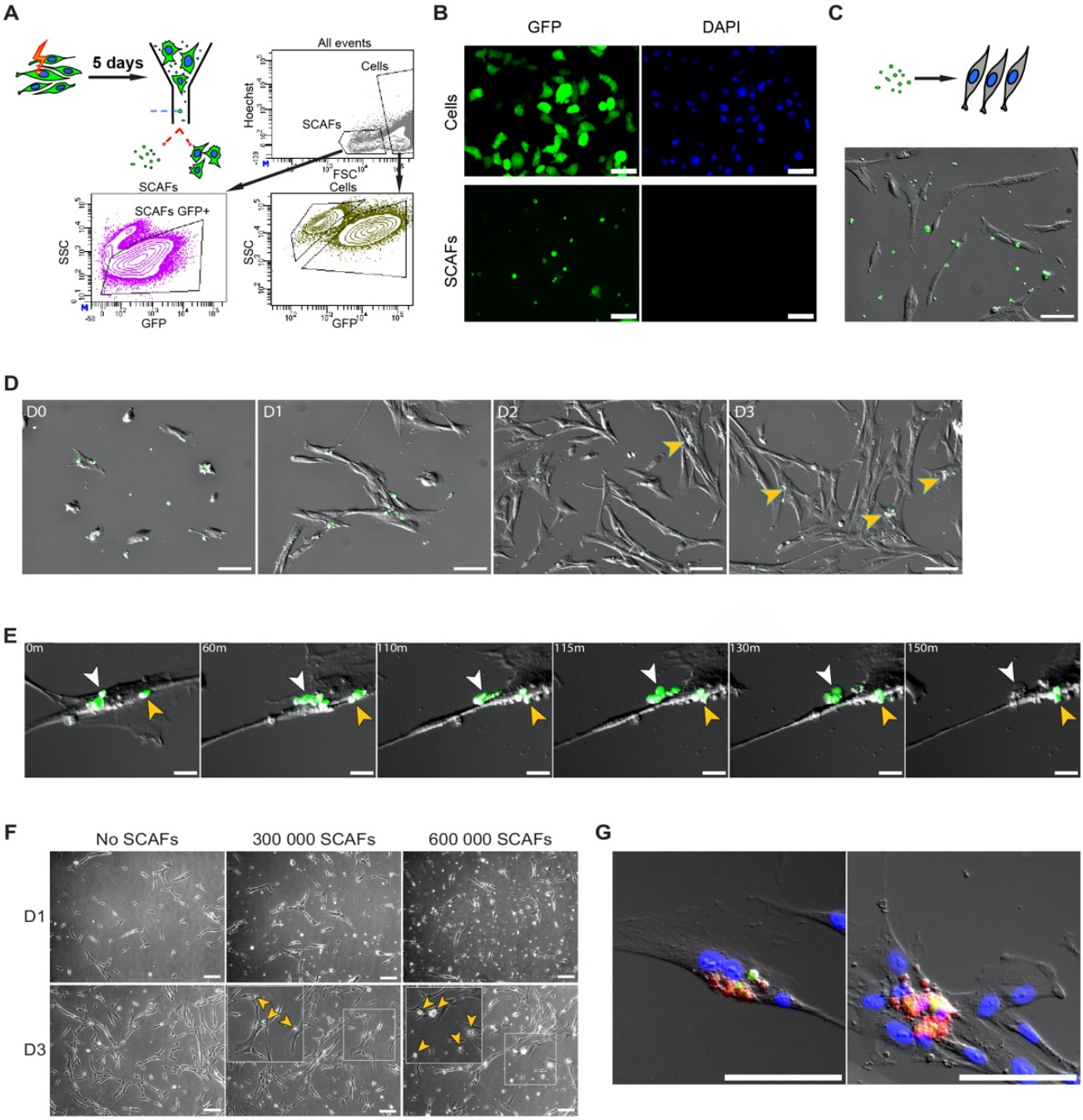
A
5 days
All events
Cells
SCAFs
Hoechst
FSC
SCAFs
SCAFs GFP+
SSC
GFP
Cells
SSC
GFP
B
GFP
DAPI
Cells
SCAFs
C
D
D0
D1
D2
D3
E
0m
60m
110m
115m
130m
150m
F
No SCAFs
300 000 SCAFs
600 000 SCAFs
D1
D3
G

Figure 5.

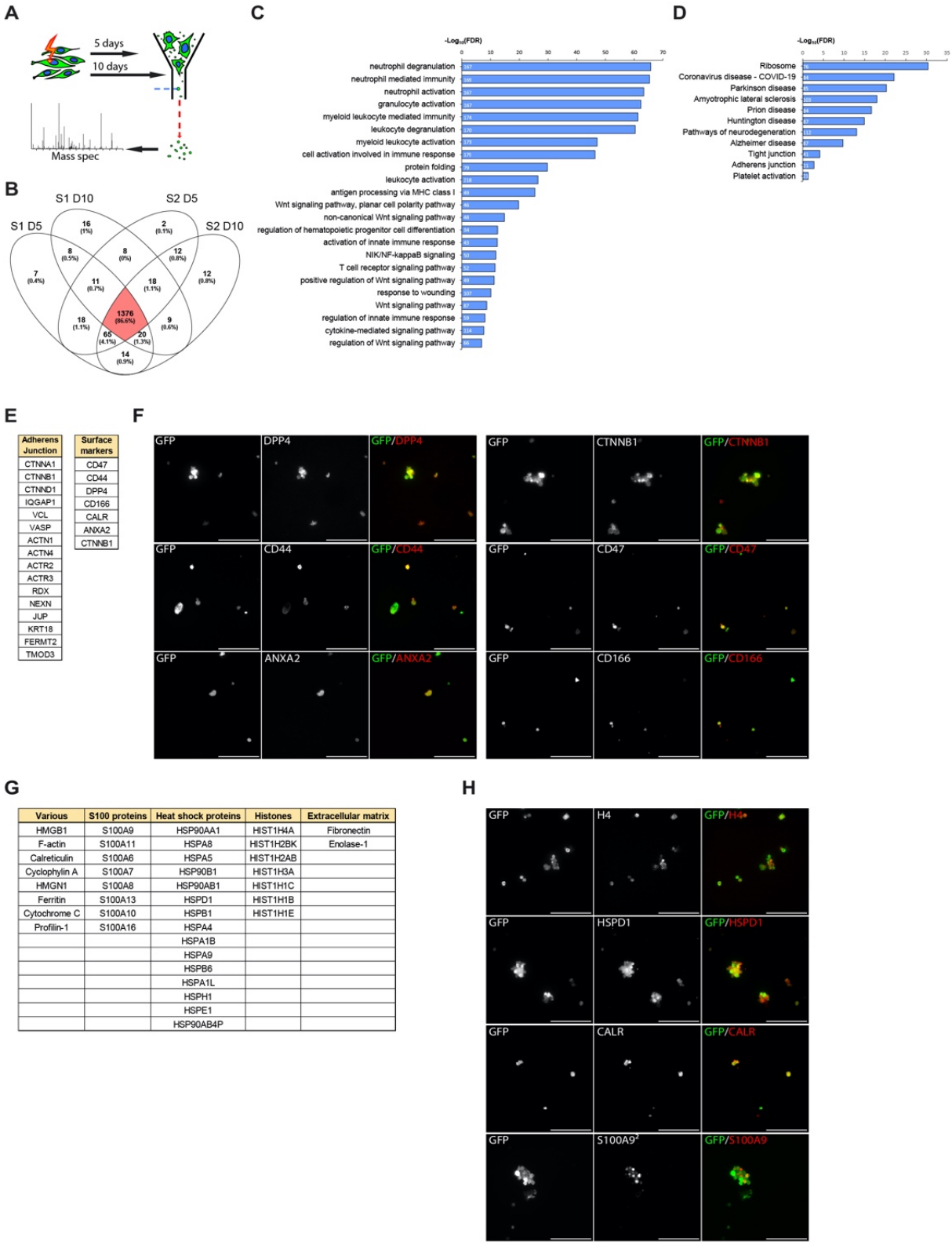

Various	S100 proteins	Heat shock proteins	Histones	Extracellular matrix
HMGB1	S100A9	HSP90AA1	HIST1H4A	Fibronectin
F-actin	S100A11	HSPA8	HIST1H2BK	Enolase-1
Calreticulin	S100A6	HSPA5	HIST1H2AB	
Cyclophylin A	S100A7	HSP90B1	HIST1H3A	
HMGN1	S100A8	HSP90AB1	HIST1H1C	
Ferritin	S100A13	HSPD1	HIST1H1B	
Cytochrome C	S100A10	HSPB1	HIST1H1E	
Profilin-1	S100A16	HSPA4		
		HSPA1B		
		HSPA9		
		HSPB6		
		HSPA1L		
		HSPH1		
		HSPE1		
		HSP90AB4P		

Figure 6.

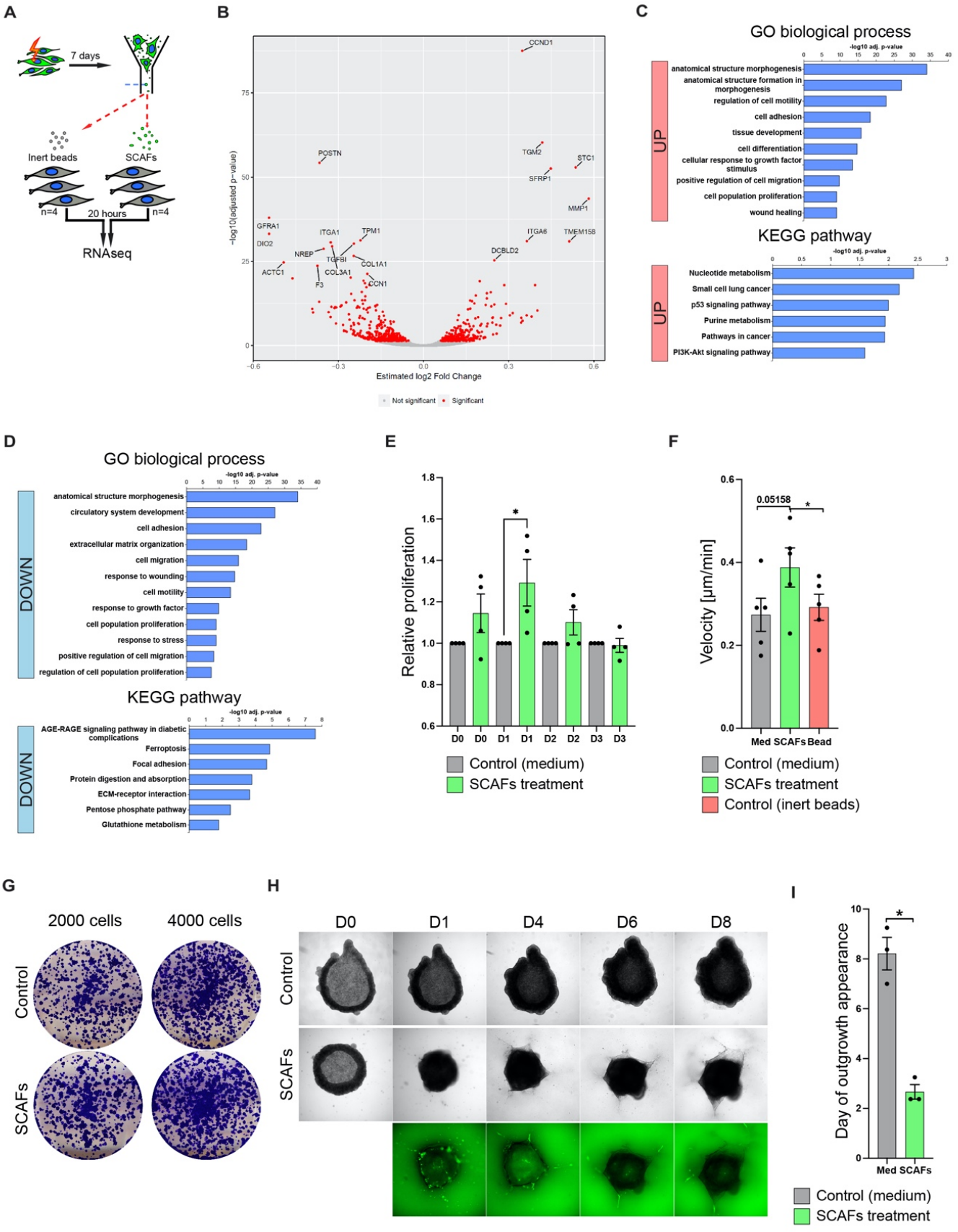
A
7 days
Inert beads
SCAFs
n=4
20 hours
n=4
RNAseq
B
CCND1
POSTN
TGM2
STC1
SFRP1
MMP1
GFRA1
DIO2
ITGA1
TPM1
NREP
TGFBI
COL1A1
COL3A1
ACTC1
F3
CCN1
ITGA6
TMEM158
DCBLD2
-log10(adjusted p-value)
Estimated log2 Fold Change
Not significant
Significant
C
GO biological process
-log10 adj. p-value
UP
anatomical structure morphogenesis
anatomical structure formation in morphogenesis
regulation of cell motility
cell adhesion
tissue development
cell differentiation
cellular response to growth factor stimulus
positive regulation of cell migration
cell population proliferation
wound healing
KEGG pathway
-log10 adj. p-value
UP
Nucleotide metabolism
Small cell lung cancer
p53 signaling pathway
Purine metabolism
Pathways in cancer
PI3K-Akt signaling pathway
D
GO biological process
-log10 adj. p-value
DOWN
anatomical structure morphogenesis
circulatory system development
cell adhesion
extracellular matrix organization
cell migration
response to wounding
cell motility
response to growth factor
cell population proliferation
response to stress
positive regulation of cell migration
regulation of cell population proliferation
KEGG pathway
-log10 adj. p-value
DOWN
AGE-RAGE signaling pathway in diabetic complications
Ferroptosis
Focal adhesion
Protein digestion and absorption
ECM-receptor interaction
Pentose phosphate pathway
Glutathione metabolism
E
Relative proliferation
D0 D0 D1 D1 D2 D2 D3 D3
Control (medium)
SCAFs treatment
F
Velocity [µm/min]
0.05158
Med SCAFs Bead
Control (medium)
SCAFs treatment
Control (inert beads)
G
2000 cells
4000 cells
Control
SCAFs
H
D0
D1
D4
D6
D8
Control
SCAFs
I
Day of outgrowth appearance
Med SCAFs
Control (medium)
SCAFs treatment

Supp. Figure 1.

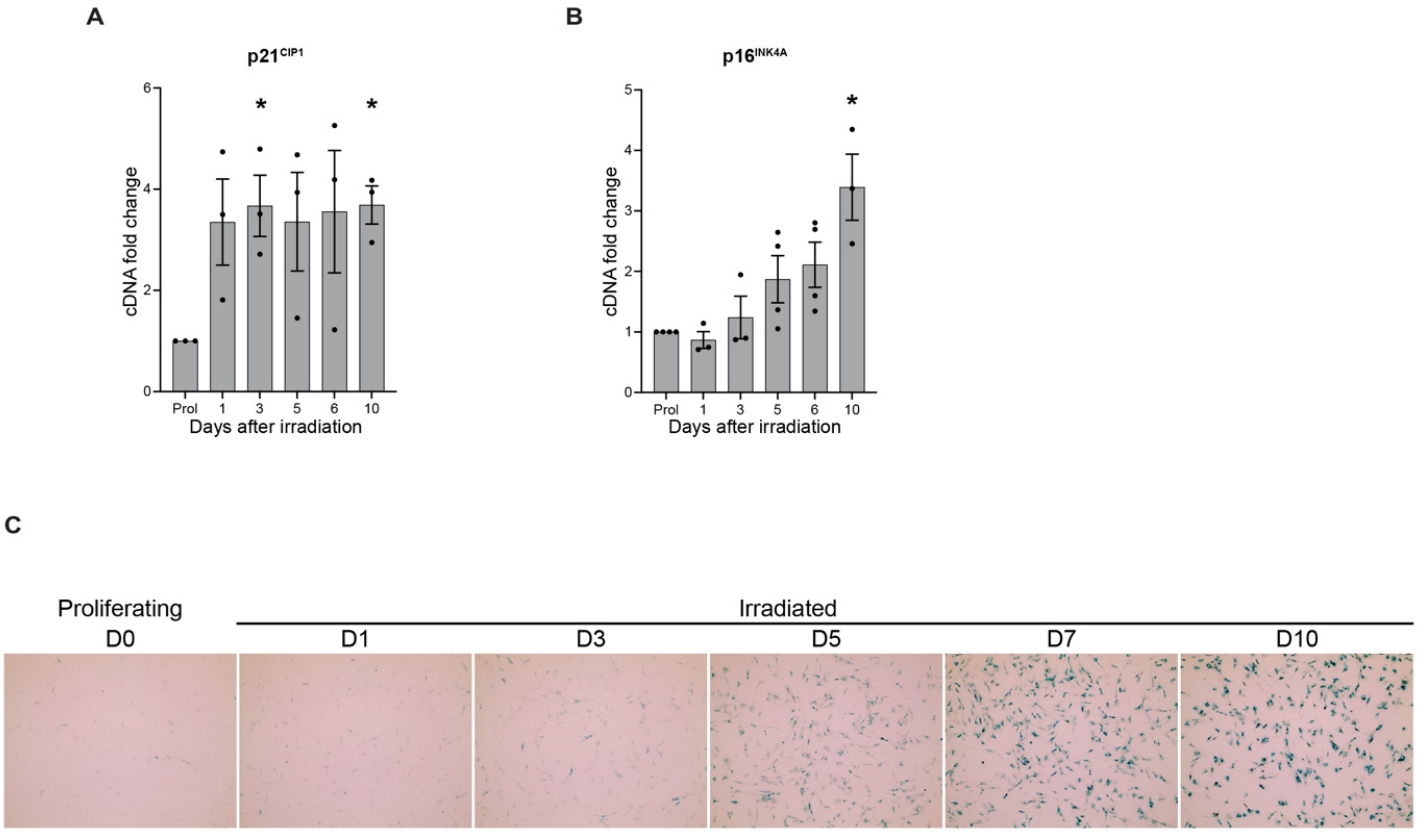
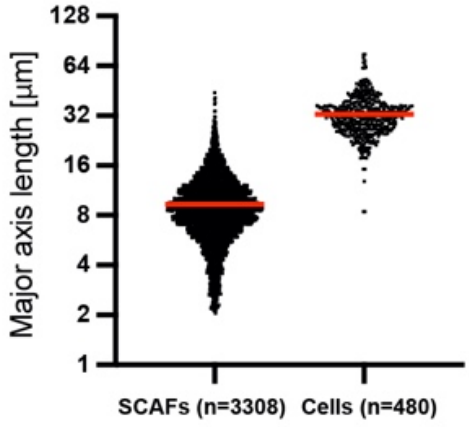
Supp. Figure 2.